Monitoring production throughout the life of unconventional and aging oil-gas wells using extended turndown ratio multiphase flowmeters

Massimiliano Fiore, SLB, Singapore
Muhammad Alif Bin Razali, SLB, Singapore
Tianhang Zhang, SLB, Singapore
Kun Yang, SLB, Singapore
Katharine Moncada, Ammar Abdelhak, Jorge Cepeda, Liviu Husoschi, SLB, USA

1 INTRODUCTION

Multiphase flowmeters (MPFMs) are essential for monitoring the flow dynamics and production of oil and gas wells across a range of gas-volume fractions (GVF) and water-liquid ratios (WLR). However, the rapid production decline and high gas output during artificial lift in unconventional wells pose significant technical challenges. Typically, MPFM sizing is based on expected initial productions, but downsizing may become necessary over time. Accurate measurement of oil and gas flow rates must be maintained, even when liquid flow rates drop below 5% of total volumetric production (i.e., GVF > 95%).
A combination of innovative solutions extends the MPFM lifespan and maintains the required accuracy throughout the life of unconventional wells, thus opening the way to the MPFM adoption to replace bulky and costly separators while providing an accurate flow rate monitoring for high-gas production.

In the US, unconventional wells exhibit a rapid and irreversible decline in production. The differential pressure (Δp) measured by MPFMs using a combination of Venturi and multienergy gamma-ray absorption can become so low that flow rate accuracy deteriorates, a situation that also affects aging conventional wells.
To avoid replacing an initially sized MPFM with a smaller one, the installation of an insert reduces the cross-sectional area at the Venturi throat, thus increasing the measured Δp for low flow rates and maintaining the measurement accuracy for low productions. This solution can be enhanced with an advantageously modified radioactive source that generates additional lower-energy X-ray emissions through X-ray fluorescence (XRF), improving sensitivity in differentiating oil from water in high GVF and high WLR flows. This increases the turndown ratio and mixture composition sensitivity, extending the MPFM's operational envelope to maintain accuracy throughout the well's lifecycle.

The lightweight and compact insert does not interfere with the X- and γ-ray beam emitted by the XRF source, thus maintaining the same photon count rates and consequently phase fraction and WLR twofold accuracy improvement. Flow rate accuracy is also preserved by an updated interpretation model that describes the multiphase flow through the new cross-sectional shape formed by the insert at the Venturi throat.
Extensive validation in a multiphase flow loop, under a wide variety of flow conditions and field tests in the US for unconventional oil-gas wells, demonstrated the twofold reduction in flow rate uncertainties for GVF > 95% compared to the MPFM with a normal source, the simple retrofit of deployed flowmeters and the robustness of the solution.

Combining the lightweight insert, called Low-rate Extender (LRE), with the XRF radioactive source in γ-ray absorption and Venturi-based MPFMs offers an effective solution for accurately monitoring production and flow dynamics throughout the lifecycle of unconventional oil and gas wells. This novel approach minimizes CAPEX utilization and reduces nonproductive time by eliminating the need for MPFM downsizing. The demonstrated accuracy and robustness of this solution in both lab and field conditions can drive increased global adoption of MPFMs, particularly in the US, replacing traditional bulky test separators equipped with natural gas-driven valves, and contributing to the achievement of sustainability goals.

After an introduction on the specificities of the flow production profile in unconventional wells, this paper describes the fit-for-basin innovations to improve the MPFM accuracy for high-gas production wells, with the XRF radioactive sources, and to maintain the measurement performance even after the rapid production decline, with the LRE. Successful cases in both laboratory and field conditions validate the technologies.

2 PRODUCTION PROFILE OF UNCONVENTIONAL WELLS, TEST SEPARATORS AND MPFM

The rapidly changing production profile of unconventional wells worldwide and in the US in particular is common for different basins (figure 1, left) and characterized by three stages (figure 1, right):

- Fracture flowback (FFB), with natural flow: The injected fluids after hydraulic fracturing are produced over a period of weeks to months, depending on the well. The formation fluids gradually displace the FFB ones, with wells typically producing naturally and reaching the maximum flowrate. Production rapidly declines down to half of the peak after less than 1 year (figure 1, left).

- Production/artificial lift (early drawdown): With largely constant fluid properties, the rapid production decline continues, with unchoked production decline rates of 60% to 80% within the first year [1]. To guarantee liquid production, artificial lift methods such as submersible pumps or gas lift are required. Along with a drop of the line pressure typically down to less than 10 bar (145 psi), gas lift methods increase the GVF well beyond 90%.

- Artificial lift (late drawdown): Assisted by artificial lift techniques, production stabilizes down to approximately 10% of the maximum flow rates recorded during the FFB stage. The increased rate of injected gas further increases the average GVF, eventually reaching > 99%. The well's life is extended through artificial lift methods, thus delaying the plugging and abandonment (P&A) of the well.

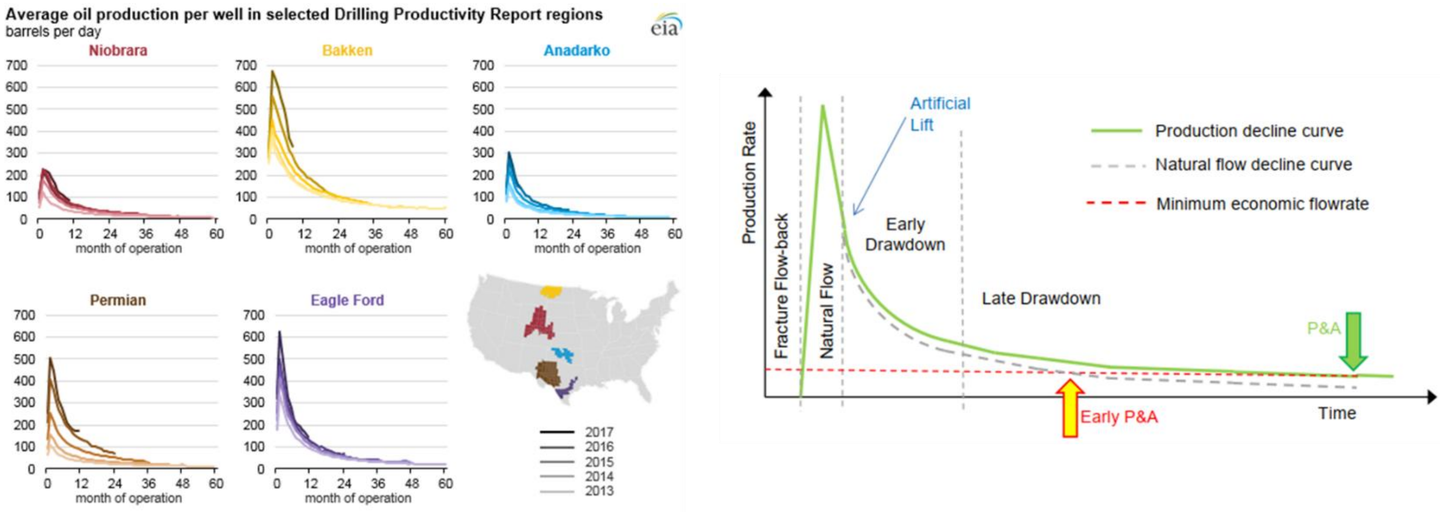

Figure 1 - Average oil production evolution from unconventional wells from 2013 to 2017, for different US basins (left [2]). Typical production decline curve for unconventional wells (right [3]).

Test separators have historically been the preferred devices to monitor well productions in the US. After gravity separation, the individual flow rates are measured with single-phase flowmeters such as Coriolis, turbines and orifice plates. This method can be reliable and accurate if the test separator is correctly sized and set up for the various flow regimes, the single-phase flowmeters are regularly maintained and inspected, and if retention time is adequate [4]. For unconventional resources, the rapid production decline represents a challenge for test separators that may become oversized for the actual production. For low flow rates, the retention time in a large volume vessel increases, thus leading to possible liquid contamination and performance degradation [5,6]. Moreover, the typical slugging nature of the flow of unconventional wells cannot be observed using a test separator due to the liquid dwell time in the separator [4]. This greatly limits the characterization of the well flow dynamic, crucial information for optimizing artificial lift strategies [7]. The large footprint at the well pad and environmental issues related to leaks and natural gas venting are other challenging aspects of test separators that operators must face.
With continuous inline measurements at high time resolution sample rates (at 1 Hz or less), smaller footprint, no natural gas vented to the atmosphere, and a 50% CAPEX reduction per well pad by simplifying

equipment, pipeline infrastructure and the investment cost for ancillaries (space, power, manifolds, etc.) [5], compact MPFMs represent an alternative way to test separator for monitoring well productions.

Since their first field deployment in early 1990s, the adoption of MPFMs has been increasing worldwide for a wide range of applications, from subsea to surface wellheads, including exploration and appraisal to production, to fiscal allocation of oil and gas fields [8]. Among the different technologies adopted for MPFMs [9], the combination of a venturi tube for total flow rate and γ-ray absorption for phase fractions of oil, water and gas has proven to be one of the most reliable in the field of multiphase flow metering, and MPFMs with this technology have been used in operations for more than 20 years. Being independent of emulsions or foaming flows, the phase fraction measurement through γ-ray absorption guarantees good measurement accuracy for production monitoring from gas- and plunger-lift techniques, as well as wet-gas unconventional wells, typically featuring an average GVF > 95%. Indeed, even when the radioactive-based measurement is considered optional, it becomes compulsory for GVF > 90% [10].
Either naturally or through artificial lift methods, most oil and gas wells eventually reach a production stage when the average GVF is larger than 90%. For conventional oil wells, this generally occurs after more than 10 years. However, for unconventional wells, the average GVF becomes larger than 90 % after only 1 or 2 years, with a rapid decline in production (figure 1).

Modeling the low-pressure (<10 bar), high-GVF (> 95%), high-WLR (typically > 60%), slug flow regimes of gas-lifted unconventional wells to achieve accurate oil flow rate measurements represents a challenge for MPFMs. The expected accuracy level throughout the life of the fast-changing GVF-increasing production of unconventional wells or aging conventional wells can be obtained with a partial gas extraction/separation to decrease the mixture GVF [11]. However, a phase splitter is generally cumbersome and costly. Increasing the oil-water attenuation contrast of X-rays emitted by a modified radioactive source represents an innovative approach for maintaining the required oil flow rate accuracy for high GVFs with a seamless upgrade of compact standard MPFMs. Combining this innovation with an insert which, when deployed in the Venturi, advantageously reduces the cross-sectional area of the Venturi throat to increase the differential pressure at low flow rates, represents a reliable solution for maintaining the required oil flow rate accuracy throughout the lifecycle of unconventional wells.
In the following sections, the theory of X- and γ-ray absorption uncertainty in MPFMs is presented, as well as the XRF physical phenomenon generating the required new energy level for an increased oil-water attenuation contrast. The dependency of the interaction length of X- and γ-rays with the multiphase flow on the measurement uncertainty is also discussed. The new XRF radioactive source is described as well as the uniquely shaped LRE insert for low flowrates. The extensive test results in both laboratory and field conditions demonstrate the robustness of the solutions and the improvement in oil flow rate performance, thus validating the upgraded MPFM as a qualified flow rate meter device throughout the entire life of unconventional wells.

3 PHASE FRACTION MEASUREMENT UNCERTAINTY THROUGH X- AND γ-RAY ABSORPTION

As detailed in [12], the phase fraction measurement in Venturi/γ-ray absorption MPFMs is based on the attenuation of X- and γ-rays after interaction with the oil-gas-water multiphase flow. The attenuation of photons by a medium obeys the Beer-Lambert law

$$n = n_0 \exp(-\lambda\, d) \tag{1}$$

where n and n_0 are the count rate (the number of photons transmitted per unit of time) after interaction and incident to the medium, respectively; λ is the linear attenuation coefficient, which depends on the incident photon energy and the medium; d is the photon-medium interaction distance.
For three-phase MPFMs to measure phase fraction based on γ ray absorption, at least two photon energies must be used and properly selected to have enough contrast between λ_o, λ_g, and λ_w, the linear attenuation coefficients of the produced oil, gas, and water, respectively. The linearity of the linear attenuation coefficient with the mixture composition allows to write the mixture linear attenuation coefficient as $\lambda_m = \alpha_w\lambda_w + \alpha_o\lambda_o + \alpha_g\lambda_g$, where α represents the fraction of the phases in the mixture. Knowing that the pipe is always filled by a water-oil-gas mixture (i.e., $\sum_{i=w,o,g}\alpha_i = 1$), the unknown phase fractions are determined by solving the following system of linear equations:

$$\begin{cases} n_{LE} = n_{0,LE} \exp\left(- \sum_{i=w,o,g} \alpha_i \lambda_{i,LE} \cdot d \right) \\ n_{HE} = n_{0,HE} \exp\left(- \sum_{i=w,o,g} \alpha_i \lambda_{i,HE} \cdot d \right) \\ \sum_{i=w,o,g} \alpha_i = 1 \end{cases} \tag{2}$$

where the subscripts LE and HE denote the two photon energies, low-energy and high-energy, properly selected to guarantee that the above equations are linearly independent. Considering the definition of the mixture linear attenuation coefficient, the Beer-Lambert law (1) also reads $\lambda_m = \frac{1}{d} \ln\left(\frac{n_0}{n}\right)$, and the phase fraction linear system can be rewritten in matrix form as follows:

$$\underbrace{\begin{pmatrix} \lambda_{w,LE} & \lambda_{o,LE} & \lambda_{g,LE} \\ \lambda_{w,HE} & \lambda_{o,HE} & \lambda_{g,HE} \\ 1 & 1 & 1 \end{pmatrix}}_{\mathbf{M}} \cdot \underbrace{\begin{pmatrix} \alpha_w \\ \alpha_o \\ \alpha_g \end{pmatrix}}_{\boldsymbol{\alpha}} = \underbrace{\begin{pmatrix} \lambda_{m,LE} \\ \lambda_{m,HE} \\ 1 \end{pmatrix}}_{\boldsymbol{\lambda}} \tag{3}$$

where the matrix $\mathbf{M}$ is obtained prior to MPFM normal operations by performing in-situ γ-ray absorption measurements of static monophasic samples of the produced fluids; $\boldsymbol{\alpha}$ contains the unknown phase fractions; $\boldsymbol{\lambda}$ includes the real-time measurements of the mixture absorptions, calculated from the measured number of photons transmitted per unit of time after interaction and incident to the medium, for two different energy levels, and from the known medium thickness (i.e., the Venturi throat diameter for Venturi-based MPFMs). To solve the linear system (3), the matrix $\mathbf{M}$ must be invertible (i.e., the rows must be linearly independent). This condition is fulfilled by properly selecting the X- and γ-ray emitting radionuclide and its energies, to have sufficient absorption contrasts between the fluid absorptions.

The ^{133}Ba radionuclide is a good candidate as X- and γ-ray emitter for MPFM applications. Out of the more than 10 naturally emitted energy levels, 2 energies can be suitably selected for the phase fraction calculation. LE at ~ 32 keV, combination of several lines between 31 and 35 keV, is sensitive to the fluid composition and thus contributes mostly to differentiating the two liquids and ultimately to measuring the "phase-fraction" ratio $WLR = \frac{\alpha_w}{\alpha_w + \alpha_o}$. HE at 81 keV mostly contributes to distinguishing the gas from the liquids. This is shown in figure 2a, also highlighting the most probable γ-ray-matter interaction phenomena: photoelectric effect for LE photons, depending on the mass attenuation coefficients of the media, and Compton scattering for HE photons, depending on density. The linear attenuation coefficients of the fluid phases populating the matrix $\mathbf{M}$ in (3) can be represented on a λ_{LE} vs λ_{HE} graph to obtain what is typically called the attenuation triangle (figure 2b); all the possible mixtures of the same compositions in single-phase oil, gas, and water will lie within the triangle area.

Unavoidable sources of uncertainty in all nuclear measurements are the statistical fluctuations inherent to the random radioactive decay process. Being described by the Poisson distribution [13], the count rate n, measured without loss of generality in s^{-1} and defined as number of measured X- and γ-rays n transmitted by a radioactive source per second and acquired over the time t (in s), is affected by the uncertainty

$$\sigma_n = \sqrt{(n/t)} \tag{4}$$

This measurement uncertainty propagates to the linear attenuation coefficients, phase fractions, and, ultimately, to the flow rates. By focusing on the phase fractions, both matrixes $\mathbf{M}$ (in-situ absorption measurements of static monophasic samples of the produced fluids) and $\boldsymbol{\lambda}$ (absorption measurement of the mixture) in (3) are affected by the uncertainty of the measured count rates. In general, by solely propagating the count rate uncertainty in flowing conditions of (4), the uncertainty of linear attenuation coefficients from the Beer-Lambert law (1) reads

$$\sigma_\lambda = \frac{1}{d} \sqrt{\left(\frac{1}{n \cdot t}\right)} \tag{5}$$

By further propagating the uncertainty of the linear attenuation coefficients, the uncertainties of WLR and α_g solely due to Poisson statics read

$$\sigma_{WLR} \propto \frac{1}{d\cdot(1-\alpha_g)}\sqrt{\left(\frac{1}{n\cdot t}\right)} \quad ; \quad \sigma_{\alpha_g} \propto \frac{1}{d}\sqrt{\left(\frac{1}{n\cdot t}\right)} \tag{6}$$

From equations (6), the direct proportionality of the phase fraction uncertainties to $1/d$ may lead to the conclusion that the smaller the MPFM size, the higher the uncertainty. The statement holds true only if d corresponds to the diameter of the circular cross-sectional area of the Venturi throat. More accurately, d corresponds to the photon-medium interaction distance. This nuance in the definition of d has important implications for maintaining the same flow rate accuracy while reducing the cross-sectional area for the multiphase flow. The innovative solution implemented in MPFMs to extend their operating life even after the rapid production decline of unconventional wells is detailed in the next section.

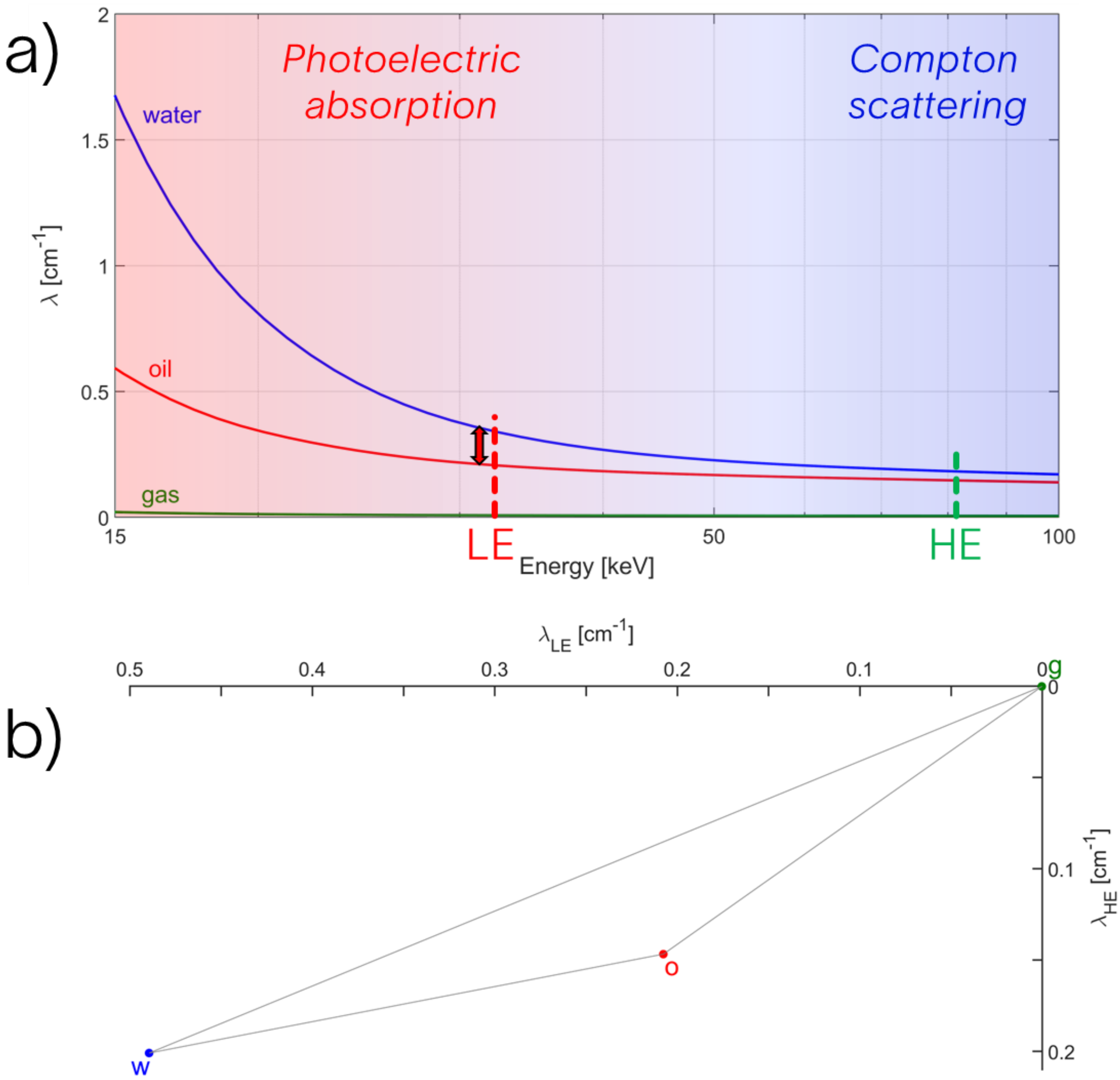

Figure 2 – a) Linear attenuation coefficient vs energy of incident photons for typical produced fluids; b) attenuation triangle.

From the WLR uncertainty (6), the denominator $(1-\alpha_g)$ becomes smaller and smaller for increasing GVF, correlated to the liner gas phase fraction through the slip law [14], which describes the relative velocity difference between gas and liquid in the multiphase flow. The WLR uncertainty naturally increases with increasing GVFs. From equations (6), the uncertainties of the phase fractions can be decreased by increasing the count rates and/or the acquisition time. Although only weakly effective (e.g., the acquisition time must be increased by a factor of 4 to halve the count rate uncertainty and finally the WLR absolute uncertainties), this would contribute to reducing the uncertainties of the (perturbed) values of both matrices $\mathbf{M}$ and $\boldsymbol{\lambda}$ in

(3). According to the perturbation theory applied to linear systems, the relative error $\frac{\|\Delta\alpha\|}{\|\alpha\|}$ of the phase fraction vector can be expressed as follows [15]:

$$\frac{\|\Delta\boldsymbol{\alpha}\|}{\|\boldsymbol{\alpha}\|} \leq \underbrace{\|\mathbf{M}^{-1}\| \cdot \|\mathbf{M}\|}_{\kappa(\mathbf{M})} \cdot \left(\frac{\|\Delta\mathbf{M}\|}{\|\mathbf{M}\|} + \frac{\|\Delta\boldsymbol{\lambda}\|}{\|\mathbf{M}\| \cdot \|\boldsymbol{\alpha}\|}\right) \tag{7}$$

where $\|\mathbf{M}\|$ is the norm of the matrix $\mathbf{M}$. The quantity $\kappa(\mathbf{M}) = \|\mathbf{M}^{-1}\| \cdot \|\mathbf{M}\|$ is the condition number of the matrix $\mathbf{M}$, measuring the relative change (or uncertainty) $\frac{\|\Delta\alpha\|}{\|\alpha\|}$ of the linear system solutions as a multiple of the relative change (or uncertainty) $\frac{\|\Delta\mathbf{M}\|}{\|\mathbf{M}\|}$ and $\|\Delta\boldsymbol{\lambda}\|$. The quantity (in brackets) multiplying $\kappa(\mathbf{M})$ will be small if the uncertainties of the values of both matrices $\mathbf{M}$ and $\boldsymbol{\lambda}$ are small, which, according to (5), can be achieved by increasing the count rates and/or the acquisition time. A radically different approach to reducing the phase fraction uncertainties is to reduce the condition number $\kappa(\mathbf{M})$. $\kappa(\mathbf{M}) = 1$ for a perfectly conditioned matrix, whereas $\kappa(\mathbf{M}) = \infty$ for a so-called ill-conditioned matrix that is singular and not invertible (i.e., the determinant $\det(\mathbf{M}) = 0$). A way to reduce $\kappa(\mathbf{M})$ is to have the rows of the matrix $\mathbf{M}$ even less linearly dependent than for an already well-conditioned matrix. For LE and HE emitted by a ^{133}Ba radioactive source, the nonlinear dependency of the attenuation matrix is guaranteed by the two different γ-ray-matter interaction phenomena dominant in the LE and HE energy regions: photoelectric absorption for LE and Compton scattering for HE (figure 2a). To increase further the nonlinear dependence of the linear attenuation coefficients at the two required energies, LE should be lower than the ^{133}Ba naturally emitted rays making up the ~ 32 keV energy level. This would drastically increase the absorption in the photoelectric domain, strongly nonlinear with the energy of the incident photon (figure 2a), thus increasing the contrast between oil and water absorptions and hence significantly improving the WLR accuracy. The innovative approach to achieving this is described in the next section.

4 MAINTAINING ACCURATE FLOW MEASUREMENT THROUGHOUT THE WELL LIFETIME

4.1 MPFM Flow Rate Accuracy Improvement at High GVF – The XRF Source

After photon absorption through the photoelectric effect (figure 3a), a photoelectron is ejected from the inner K-shell and a vacancy is created (figure 3b). The K-shell vacancy is filled by an L-shell electron, and the excess of energy is either given off as a characteristic fluorescence X-ray (figure 3c), or it can be transferred to an electron of an outer (M-) shell before escaping from an atom as Auger electron (figure 3d). The X-ray fluorescence (XRF) yield ω_k represents the probability of producing a K X-ray after the K-shell of an atom has a vacancy; on the other hand, 1-ω_k is the probability of producing an Auger electron with lower energy of fluorescence X-rays.

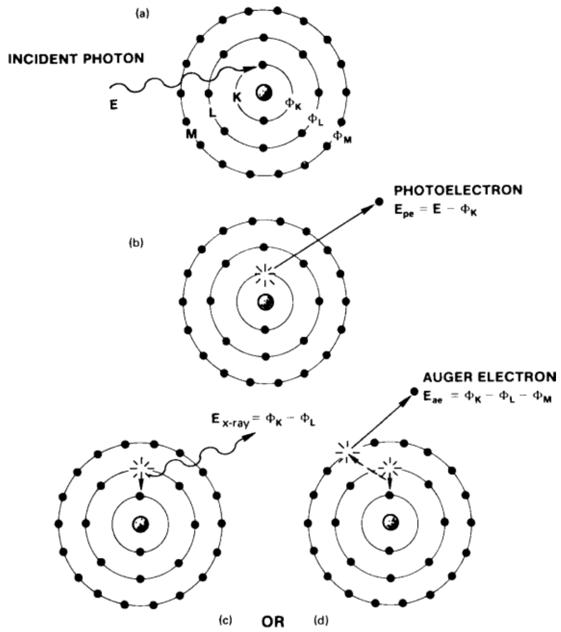

Fig. 3 – Production of characteristic fluorescence X-rays. (a) Excitation of a K-orbital electron producing a K vacancy. (b) Emission of a photoelectron producing a K vacancy. Deexcitation leads to (c) the emission of a characteristic K photon fluorescence X-rays or (d) an Auger electron [16].

By advantageously choosing an element generating a fluorescence X-ray with energy < LE (figure 2a), the ^{133}Ba naturally emitted rays making up the ~32 keV energy level can lead to an XRF emission in the range between 15 keV and 25 keV, called very low energy (VLE). The outer dimensions of the XRF source are the same as the standard ones. The internal differences are i) the insertion of an XRF metal foil at contact with the solid radioactive material and ii) making the part surrounding the radioactive material of the same fluorescence material [17]. This "fluorescence cell" surrounding the radioactive material converts a portion of LE photons into VLE X-rays; the XRF foil contributes the most to the generation of the VLE photons having the right direction towards the multiphase flow and the scintillation detector. The thickness of the XRF foil can be optimized to maximize the fluorescence X-ray emission. Indeed, two competing effects must be considered: a too thin foil would minimize the probability of interaction of the incident photons, thus generating only a few fluorescence X-rays, whereas a too thick foil would maximize the probability of interaction of the incident photons and fluorescence X-ray generation, which, however, will be absorbed by the foil itself. The optimized thickness depends on the energies of the incident photons and fluorescence X-rays, as well as on the density of the fluorescence material [18]. To guarantee a stable emission of fluorescence X-rays over time regardless of temperature changes, a metal with a low coefficient of thermal expansion and low chemical reactivity should be preferred.

The VLE fluorescence X-rays emitted by the ^{133}Ba XRF source show a much larger absorption contrast than LE does between oil and water (figure 4a). By replacing LE with VLE in the attenuation triangle, the XRF triangle defined by VLE and HE linear attenuation coefficients has a much larger area than the standard LE-HE triangle, as shown in figure 4b (note the different x-axis scale from figure 2b).

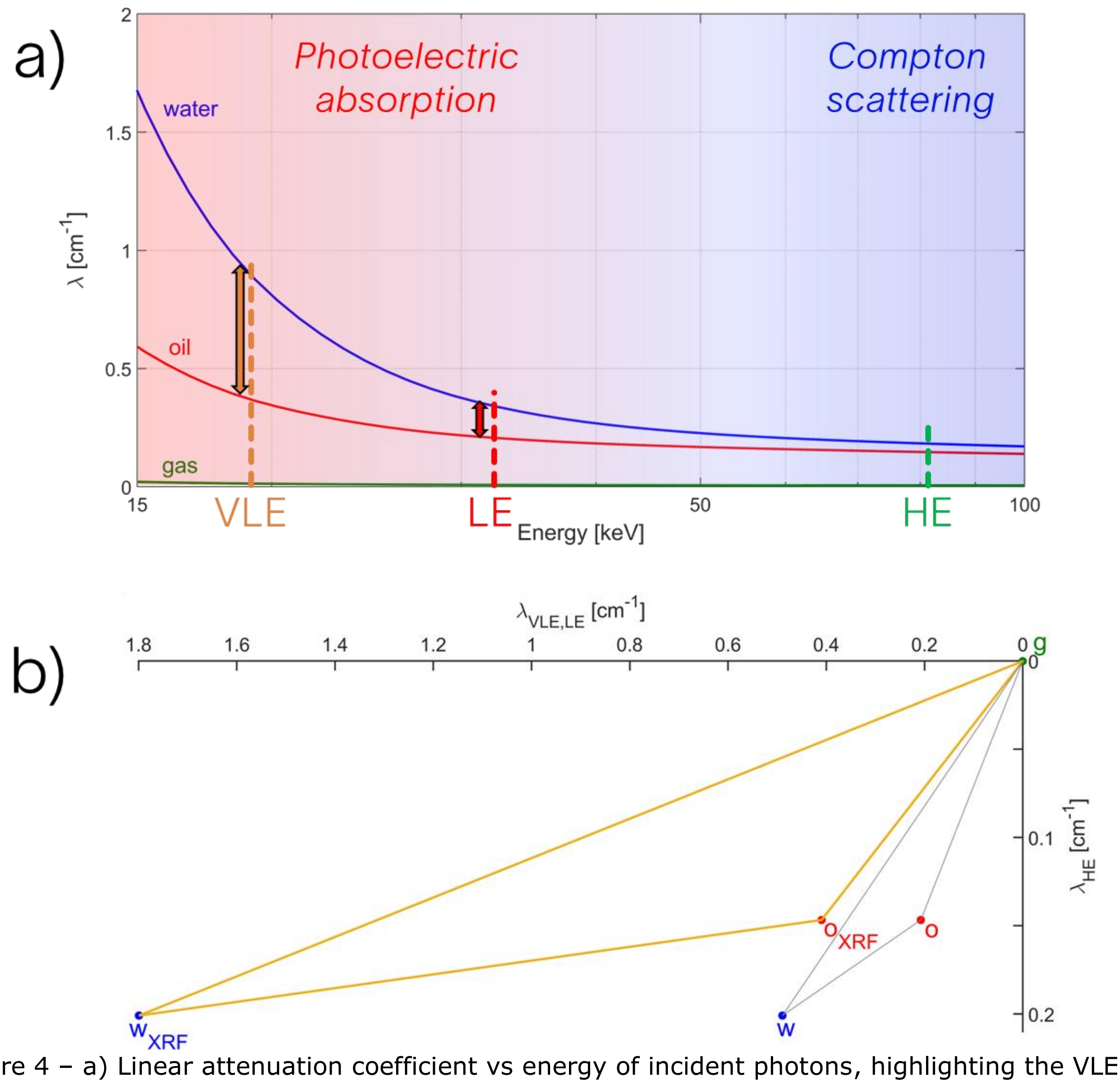

Figure 4 – a) Linear attenuation coefficient vs energy of incident photons, highlighting the VLE fluorescence X-rays, for typical produced fluids; b) XRF (orange) and standard (thin black) attenuation triangles.

In mathematical terms, the replacement of LE with VLE photons translates into a new linear system for the phase fraction calculation as follows:

$$\underbrace{\begin{pmatrix} \lambda_{w,VLE} & \lambda_{o,VLE} & \lambda_{g,VLE} \\ \lambda_{w,HE} & \lambda_{o,HE} & \lambda_{g,HE} \\ 1 & 1 & 1 \end{pmatrix}}_{\mathbf{M_{XRF}}} \cdot \underbrace{\begin{pmatrix} \alpha_w \\ \alpha_o \\ \alpha_g \end{pmatrix}}_{\boldsymbol{\alpha}} = \underbrace{\begin{pmatrix} \lambda_{m,VLE} \\ \lambda_{m,HE} \\ 1 \end{pmatrix}}_{\boldsymbol{\lambda_{XRF}}} \quad (8)$$

For typical production fluids, the ratio of the condition numbers for the attenuation matrices $\mathbf{M_{XRF}}$ and $\mathbf{M}$ is $\frac{\kappa(\mathbf{M_{XRF}})}{\kappa(\mathbf{M})} < 1$; according to equation (7), the use of the XRF source emissions guarantees an improvement of the phase fraction accuracy.

The imperfections of scintillation detectors described in detail in [19] represent a challenge for a proper extraction of the VLE emissions from the measured ^{133}Ba XRF energy spectrum. In the energy range between 15 keV and 25 keV, the peak of the XRF emissions overlaps with the escape peak of the naturally emitted emissions combined in LE (figure 5), and a standard energy window approach is not applicable. Only a full spectrum analysis can properly model the measured XRF energy spectrum obtained by combining the contributions of mono-energetic ^{133}Ba XRF source emissions properly extracted by a dedicated algorithm in real time [20]. The results of the measured XRF spectrum decomposition into the contribution of individual incident X- and γ-ray energies are shown in figure 5b, with the highlighted XRF peak properly extracted and leading to the correct VLE count rate.

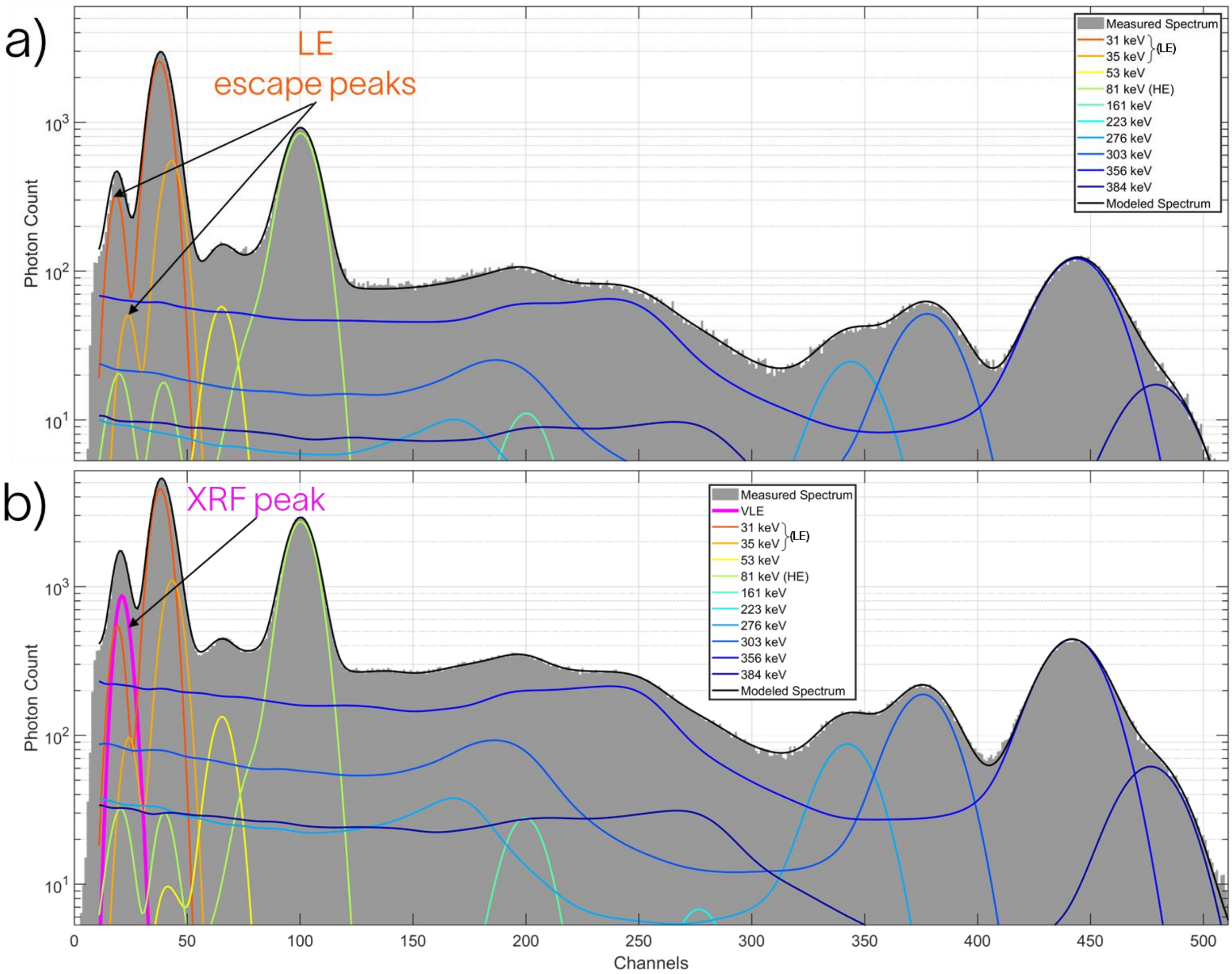

Figure 5 - Measured ^{133}Ba energy spectrum, with decomposition into the contribution of individual incident X- and γ-ray energies: a) for standard radioactive source; b) for XRF source.

For a typical MPFM size for unconventional wells, the new VLE-HE mode starts from a GVF ≥ 85% due to the high absorption of the VLE fluorescence X-rays. To maximize the VLE count rate through the XRF phenomenon, the ^{133}Ba XRF source activity is increased, while slightly adjusting the metal shielding required to keep the same low dose rate (< 1 μSv/h) at the contact of any accessible surface of the MPFM [21]. For lower GVFs, the higher-activity XRF source also leads to a small improvement in phase fraction accuracy due to the higher LE and HE count rates (5).

To obtain an accurate oil flow rate, an accurate WLR is even more important for unconventional wells, due to the typically high WLR > 60%. Indeed, from the definitions of $WLR = \frac{q_w}{q_w+q_o}$ and the liquid flow rate $q_l = q_w + q_o$, where q_w and q_o are the volumetric water and oil flow rate, respectively, the oil flow rate can be expressed as $q_o = (1 - WLR) \cdot q_l$. By propagating the absolute uncertainty ΔWLR and the relative liquid uncertainty $\frac{\Delta q_l}{q_l}$, the relative uncertainty of the oil flow rate reads

$$\frac{\Delta q_o}{q_o} = \sqrt{\left(\frac{\Delta WLR}{1 - WLR}\right)^2 + \left(\frac{\Delta q_l}{q_l}\right)^2} \qquad (9)$$

For high WLRs, the absolute WLR uncertainty is amplified by the small denominator of (9), thus emphasizing the importance of an accurate WLR for an accurate oil flow rate in typical high-WLR unconventional well conditions.

4.2 MPFM Lifetime Extension with Improved Accuracy - The Low-Rate Extender

The rapid production decline of unconventional wells can lead to the MPFM operating point outside of the operating envelope defined by the Δp sensor. Figure 6a shows the possible production condition of an unconventional well (empty green dot) in the liquid-gas flow rates graph, followed by a later production stage with less liquid and more gas (full green dot). This typical behaviour is often driven by injected gas in the artificial lift phase, which increases the average GVF while the total mass flow rate decreases. Prior to installation, the MPFM is sized according to the expected flow rates and the operating range of the Δp sensor, defined by a lower and upper limit (red curves in figure 6a). When the produced flow rate becomes so low that the corresponding Δp is smaller than the lower limit of the sensor operating range, the measured total mass flow rate Q can become inaccurate, given that $Q \propto A \cdot \sqrt{\Delta p}$, where A is the cross-sectional area of the Venturi throat (figure 6b).

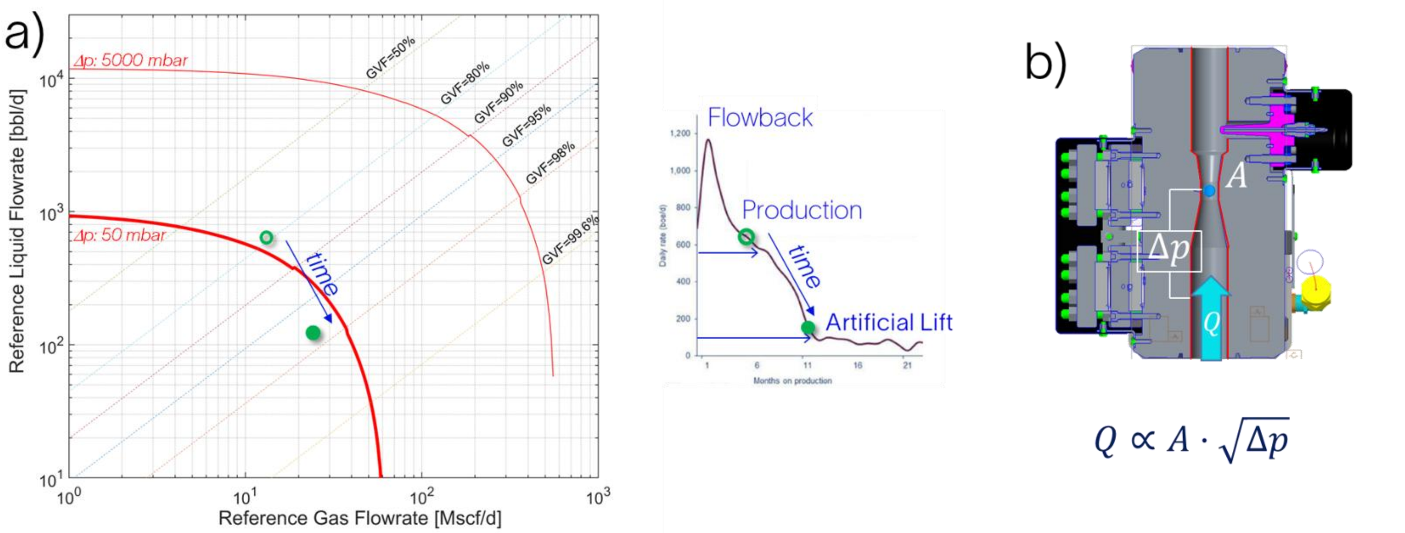

Figure 6 – a) MPFM operating envelope defined by the Δp operating range of the differential pression sensor, and example of production temporal evolution (green dots); b) MPFM cross-section highlighting in red the Venturi tube profile. The total mass flow rate Q is largely proportional to the cross-sectional area A of the Venturi throat and the square root of the differential pressure Δp.

During the artificial lift stage, MPFMs based on a Venturi tube may require a replacement with a smaller-size meter to maintain a high enough and accurate differential pressure measurement for low flow rates. As shown in figure 7a, the new MPFM operating envelope defined by the blue curves largely includes the production condition with low flow rates (green point). However, replacing an MPFM is CAPEX and operationally demanding. A different approach is to install an insert, called Low-rate Extender (LRE), in the originally installed MPFM, to create a constriction in the Venturi throat (figure 7b). According to the conservation of energy, the reduction of the cross-sectional area $A' < A$ leads to an increased differential pressure $\Delta p'$ for the same low total mass flow rate Q.

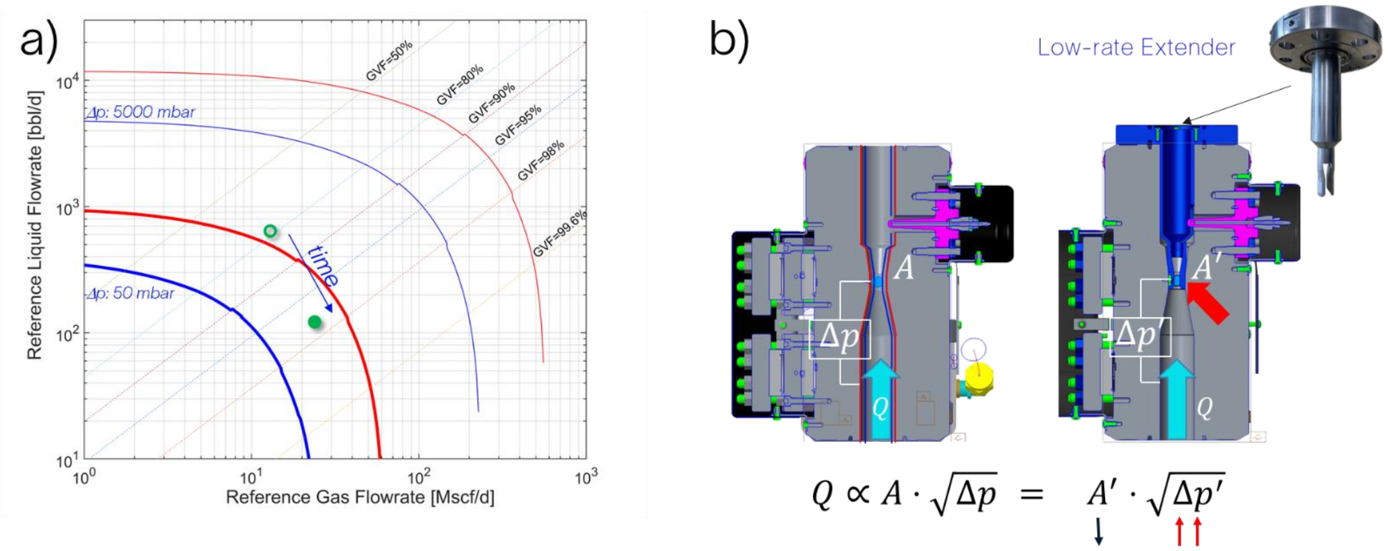

$$Q \propto A \cdot \sqrt{\Delta p} = A' \cdot \sqrt{\Delta p'}$$

Figure 7 – a) MPFM operating envelope before (red) and after (blue) downsizing; b) MPFM cross-sections highlighting in blue the downsized Venturi profile (left) and with LRE installed (right).

After the installation of the LRE, the MPFM turndown ratio TR, defined as the ratio between maximum Q_{max} and minimum Q_{min} accurately measurable flow rates, is extended by the new lower limit corresponding to the "Δp=50 mbar" blue curve in figure 8a. The TR extension factor ε_{TR} of the MPFM can be easily calculated as follows:

$$\varepsilon_{TR} = \frac{TR_{LRE}}{TR} = \frac{Q_{max}/Q_{min,LRE}}{Q_{max}/Q_{min}} = \frac{Q_{min}}{Q_{min,LRE}} \approx \frac{A}{A'} = \left(\frac{d}{d'}\right)^2 \quad (10)$$

where $Q_{min,LRE}$ is the minimum flow rate accurately measurable with the LRE installed, d and d' are the diameters of the originally installed MPFM and the downsized one, respectively, provided that the cross-sectional area at the Venturi throat is circular (figure 8a). However, with LRE installed, the cross-sectional area at the Venturi throat is not circular, due to the fork-like shape highlighted in figure 9c. This fork design allows the X- and γ-ray beam to pass through the throat as if without the LRE. Indeed, the beam width w is maintained even with the LRE installed (figures 8a and 8b), as well as the interaction distance d between X- and γ-rays and the multiphase mixture. This and equation (6) lead to the important conclusion that the accuracy improvement from the XRF source is maintained even after the LRE installation in the MPFM, throughout the life of the well. Equation (10) is valid as long as d and d' represent the diameters of the circular cross-sectional areas which equate the flow passage area of the flow, where the phase fractions are calculated, regardless of its shape.

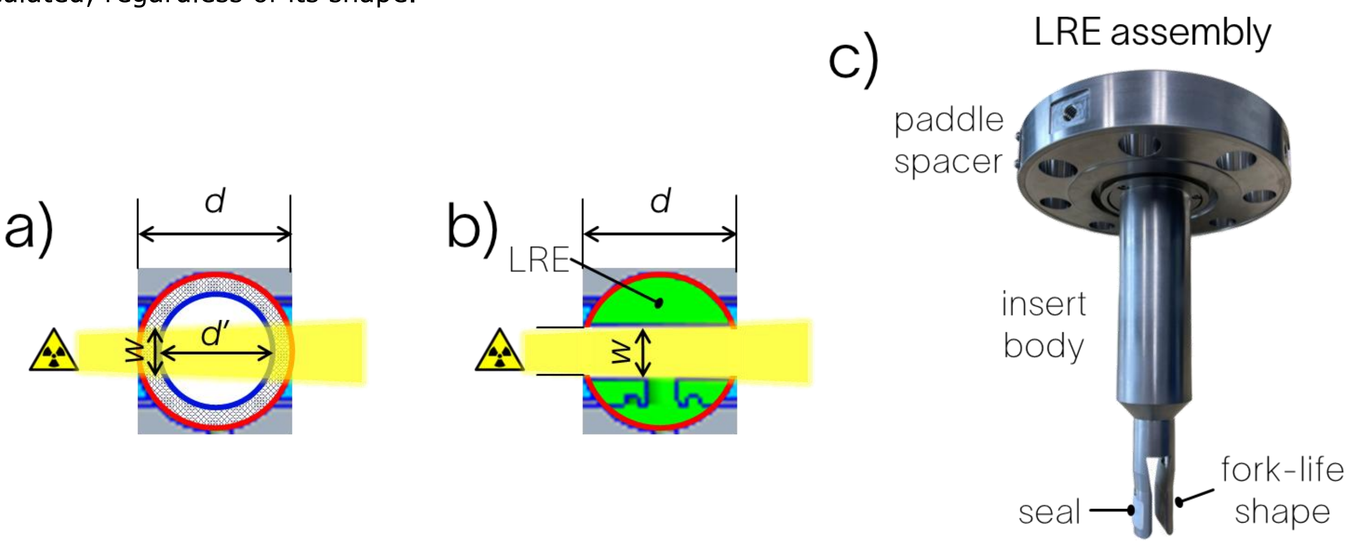

Figure 8 – a) Cross-section of the MPFM Venturi throat with downsized MPFM (from red to blue profiles); b) Cross-section of the MPFM Venturi throat with LRE installed; c) LRE assembly.

The LRE assembly in figure 9c features three main parts:

- the pressure-retainer paddle spacer - It secures the assembly by locking it into place, while guaranteeing the alignment of the fork-like shape with the X- and γ-ray beam as well as with the pressure port;

- the insert body – It connects the paddle spacer and the fork-like section in the Venturi throat by creating the constriction for the turndown ratio increase;

- the seal – It prevents the multiphase mixture to flow between the outside of the LRE and the inner surface of the Venturi tube, so that the pressure measured at the port it seals correctly corresponds to the one created by the total mass flow rate of the multiphase mixture.

5 TEST RESULTS

Topside MPFMs equipped with XRF sources and LRE were extensively tested in both flow loop and field conditions. More than 1,500 test points with several mixtures at different flow rates, line pressures and water salinities were captured to demonstrate the improvement in oil flow rate accuracy with a focus on typical unconventional well conditions with high WLR and high GVF. The usability and robustness of the XRF radioactive source and the LRE solutions were demonstrated in field conditions for several unconventional wells in the Permian basin, Texas, US. The accuracy improvement of the oil flow rate was also demonstrated against reference measurements from single-phase flowmeters used in test separators and a lease automatic custody transfers (LACT) unit.
For both flow loop and field tests, MPFMs with 29-mm diameter Venturi throat were employed, with LREs converting them into an almost-rectangular flow passage area equivalent to a 19-mm diameter circular cross-sectional area at the throat. According to equation (10), in these cases the MPFM TR is extended by a factor of $(29/19)^2 = 2.33$, corresponding to a Δp increase factor for the same mass flow rate of (see figure 8b):

$$\frac{\Delta p'}{\Delta p} = \left(\frac{A}{A'}\right)^2 = \left(\frac{d}{d'}\right)^4 = \left(\frac{29}{19}\right)^4 = 5.43 \qquad (11)$$

Flow rate measurement results in flow loop and field test conditions are presented in this section.

5.1 Laboratory Results in Flow Loop

Because of their high-accuracy references and controlled conditions, tests using ISO-accredited multiphase flow loop facilities represent the most reliable way to evaluate the performance of MPFMs by circulating mixtures of oil, water and gas at various flow rates and pressures. Figure 9 shows the schematic and test setup at the SLB Singapore Well Testing Center (SWTC) multiphase flow loop facility, where an MPFM equipped with a standard ^{133}Ba radioactive source and LRE is installed upstream of an identical MPFM equipped with a ^{133}Ba XRF source and LRE. The XRF source assembly is fully compatible with the standard MPFM main body for a seamless upgrade. The closed flow loop facility consists of a three-phase separation system, a gas compressor, two liquid pumps, and a set of high-precision reference flowmeters on each single-phase line. After the mixing point, the multiphase flow passes through the MPFMs under test and finally returns to the separator. Comparing the MPFM flow rates with the reference flow rates allows the assessment of the MPFM performance to a high degree of accuracy. More than 1,500 test measurement points with several mixtures at different flow rates, line pressures and water salinities were captured, with a particular focus on typical unconventional well conditions: low line pressure of ~10 bar, from fresh water to medium water salinities up to 10%-NaCl mass concentration, Exxsol D80 synthetic oil, and high-WLR and high-GVF mixtures. It is important to note that the individual flow rates of each one of the measurement points are averaged over relatively short acquisition periods, from 5 to 30 minutes, depending on the GVF (the higher the GVF, the longer the acquisition period). In those conditions, the unavoidable nuclear measurement uncertainty of equation (6) plays a non-negligible part, especially for high-GVF mixtures.

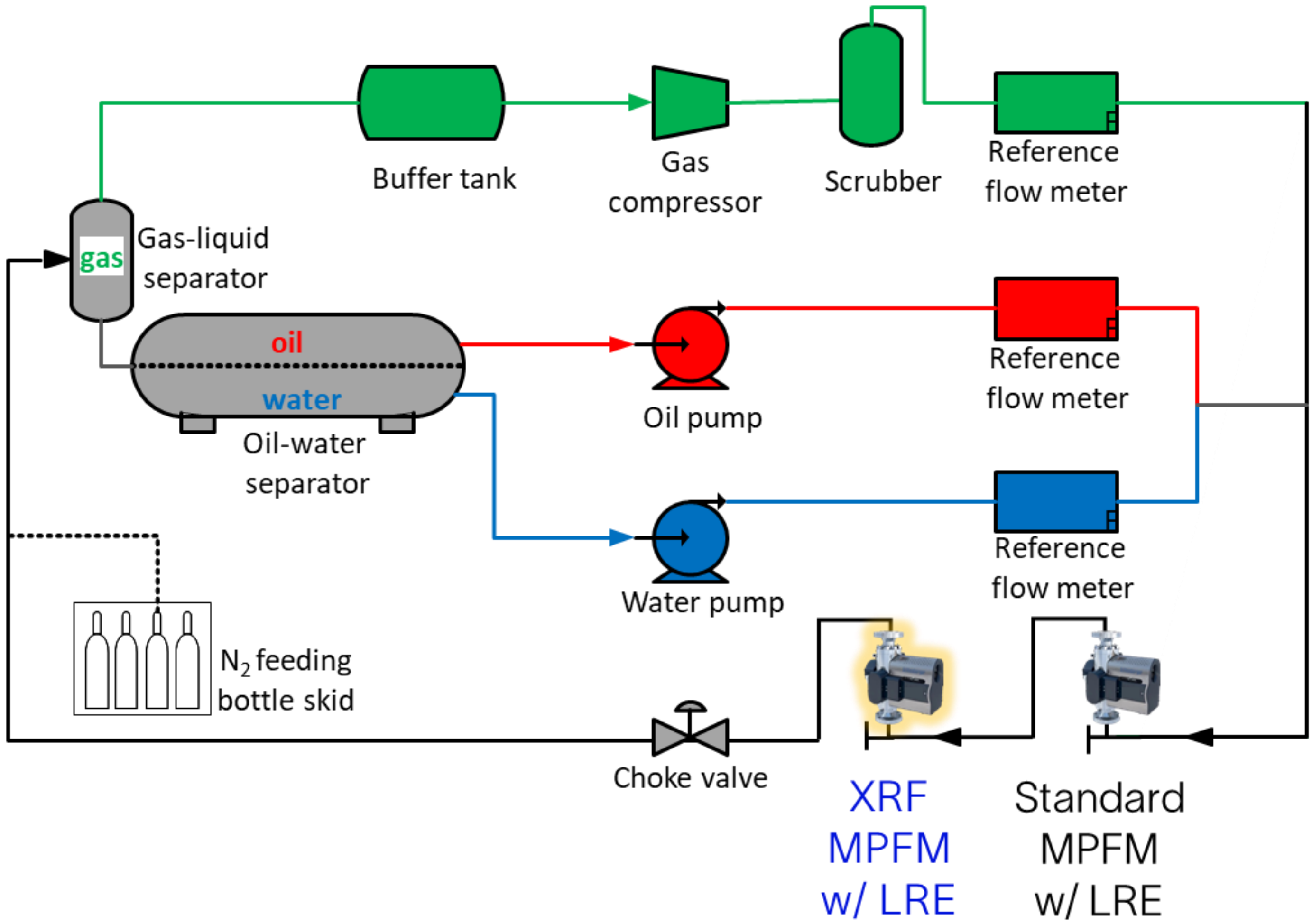

Figure 9 – Schematic of the SWTC flow loop. MPFM equipped with XRF source and LRE downstream a standard MPFM with LRE.

Figure 10 shows a summary of the flow loop oil flow-rate test results, with a comparison between the standard and the XRF MPFMs. All the possible mixtures of the oil, gas, and water flowing in the flow loop are within the area of the WLR-vs.-GVF mapping. The 50%-oil 50%-gas and 50%-water 50%-gas water points are highlighted in yellow (top left corner) and in cyan (bottom left corner), respectively. Moving along the horizontal line from left to right, the GVF in the mixture increases, for the same WLR; on the other hand, moving along the vertical axis, the WLR increases from top to bottom, for the same GVF. The mixtures tested in flow loop correspond to the small blue points; the same mixtures, defined by WLR and GVF, were tested multiple times at different line pressures, flow rates (i.e., differential pressure) and water salinities. The accuracy of the oil flow rate mapping is based on the colorbar on the right of figure 10 and represents the relative deviation of the oil flow rate averaged over the measurement point acquisition time from the highly accurate reference measured by single-phase Coriolis meters in the oil line. The accuracy improvement of the oil flow rate is clearly shown by a wider green area for the XRF MPFM, especially for unconventional well conditions at high WLR and high GVFs. This improvement originates from an absolute WLR uncertainty reduction by a factor > 2 for GVF > 95% from the use of the VLE X-ray emission from the ^{133}Ba XRF source (see figure 4a).
The same flow loop test results were obtained with standard and XRF MPFMs with LRE installed. As explained in section 4.2, the special design of the LRE does not change the phase fraction calculation accuracy. The accuracy of the individual flow rates is maintained with an updated multiphase flow model which, although nonconforming to the Venturi tube ISO standard [22], properly considers the non-circular geometry of the Venturi throat with the LRE installed

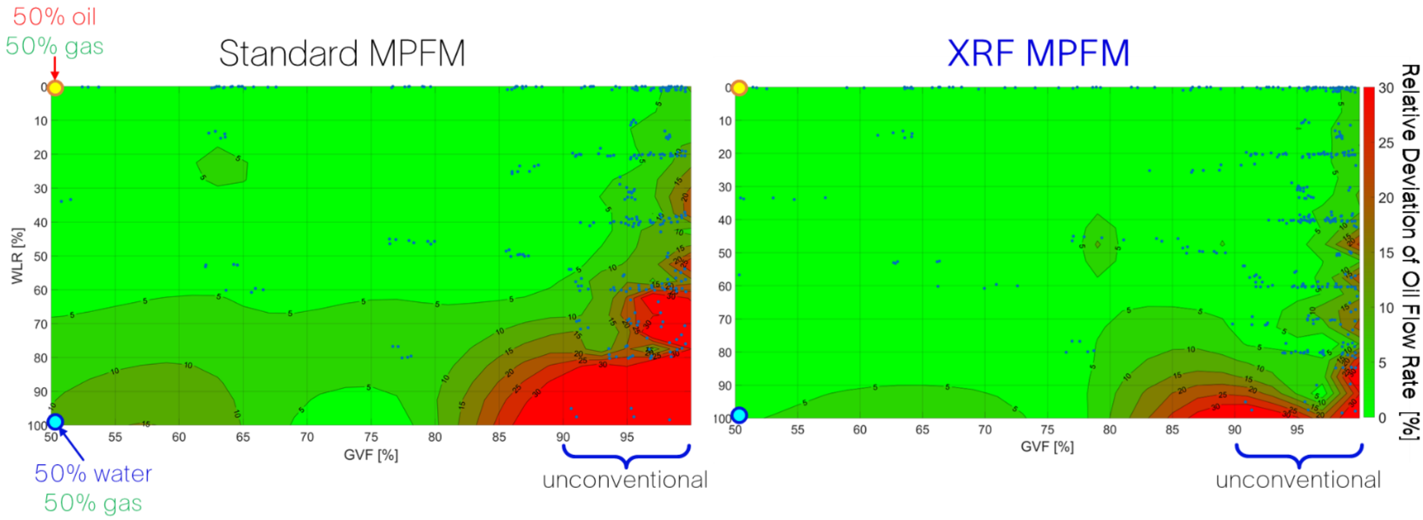

Figure 10 – Flow loop test results: oil flow rate relative deviation as measured by the standard (left) and the XRF (right) MPFM. Same results are obtained when an LRE is installed in the MPFMs.

5.2 Field Deployment and Results

Several MPFMs equipped with the ^{133}Ba XRF source have been deployed in the Permian basin, Texas, US, to validate the robustness of the solution and the flow rate accuracy improvement for unconventional well conditions. Already deployed MPFMs in the production and artificial lift stages (see figure 1) were seamlessly upgraded by replacing the standard source with the XRF one, fully compatible with the standard MPFM main body, as well as by upgrading the software including the XRF energy spectrum interpretation model (see figure 5). Six wells were tested with the XRF MPFM, with average GVF from 98% to 99.3% and average WLR from 25% to 97% for a total of 420 days of combined test duration [11]. The XRF MPFM flow rates were compared with the output from test separators equipped with single-phase flowmeters taken as reference measurements: either turbine or Coriolis meters for the oil line, turbine or electromagnetic flowmeters for the water line, and orifice plates for the gas flow rate.
The unavoidable nuclear measurement uncertainty of equation (6) propagates to the flow phase fractions and to the WLR, which is illustrated in figure 11 for a 99.1%-GVF well. Despite the fluctuations due to the highly unstable flow, once the MPFM is upgraded to the XRF source and the corresponding data interpretation mode, the amplitude of the 5-minute averaged WLR fluctuations is halved, in agreement with the flow loop test results shown in figure 10.

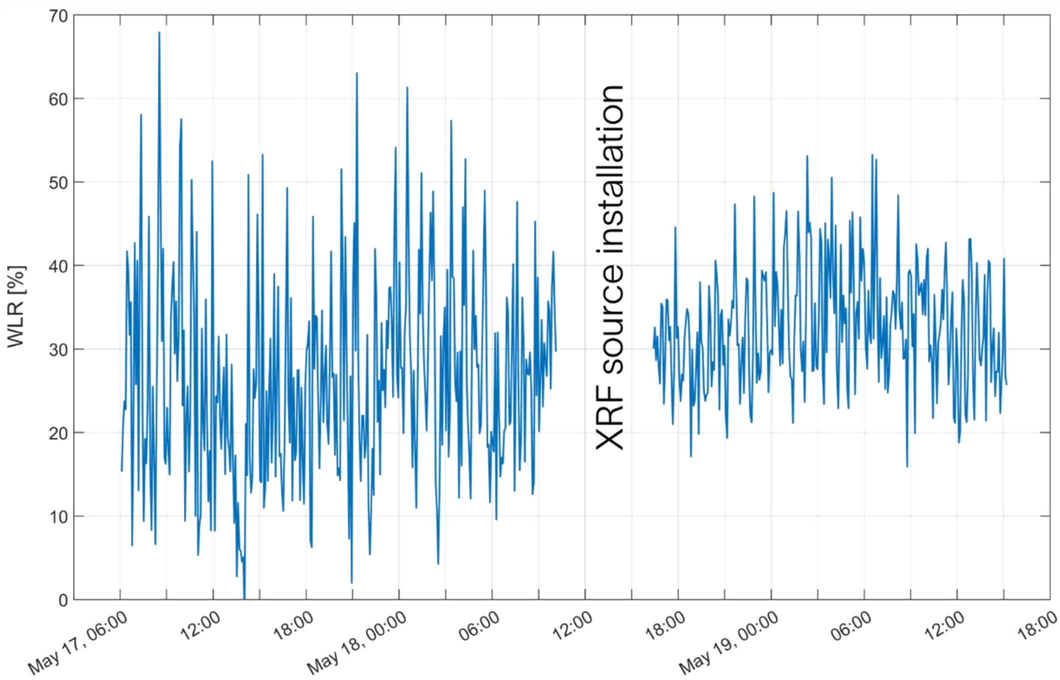

Figure 11 – WLR from MPFM (5-minute averaged) in field conditions at 99.1% GVF: before and after the installation of an XRF source. The standard deviation of the WLR is roughly halved with the XRF source.

Figure 12 shows the oil flow rate evolution of the 99.1%-GVF 30%-WLR well (see figure 11), and reference measurement from an accurate LACT unit equipped with a Coriolis meter for the oil line after separation. Each point corresponds to the daily cumulative oil production The stable oil production measured by the LACT unit is measured with a relatively large uncertainty by the standard MPFM. However, except for the events on 28 May and 29 May due to an issue in the reference readings as confirmed by the oilfield owner, the oil flow rate is well within the 10% error bars from the daily production measured by the XRF MPFM, thus demonstrating the important accuracy improvement.

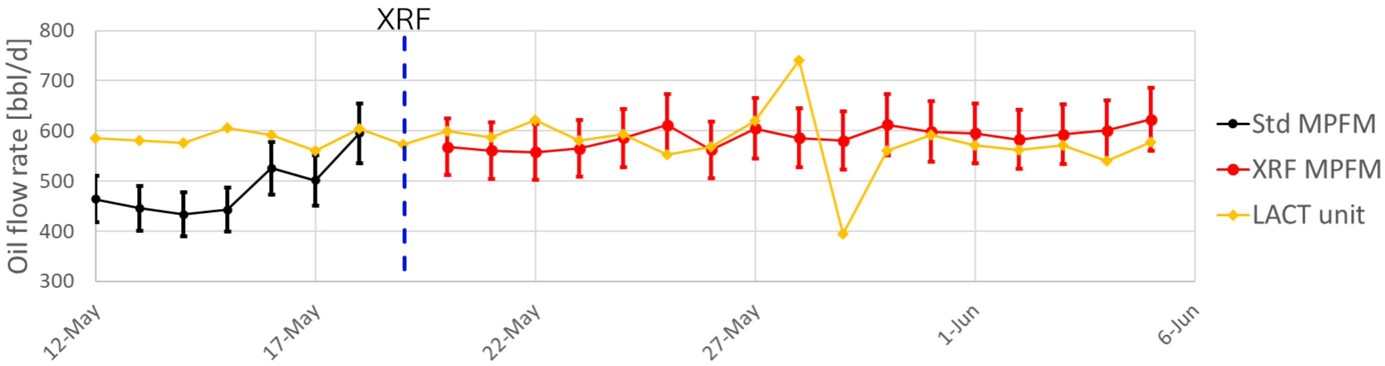

Figure 12 – Oil flow rate from MPFM before and after the installation of an XRF source, for WLR ~30% and 99.1% GVF. Error bars show the ±10% relative uncertainty of the daily production. Reference measurements from LACT unit.

Figure 13 shows a typical installation of the MPFM equipped with XRF source and LRE for monitoring the production of unconventional wells. Two more wells were tested with XRF MPFMs and LRE, with average GVF from 92% to 97% and average WLR from 13% to 35% for a total of additional 200 days of combined test duration.

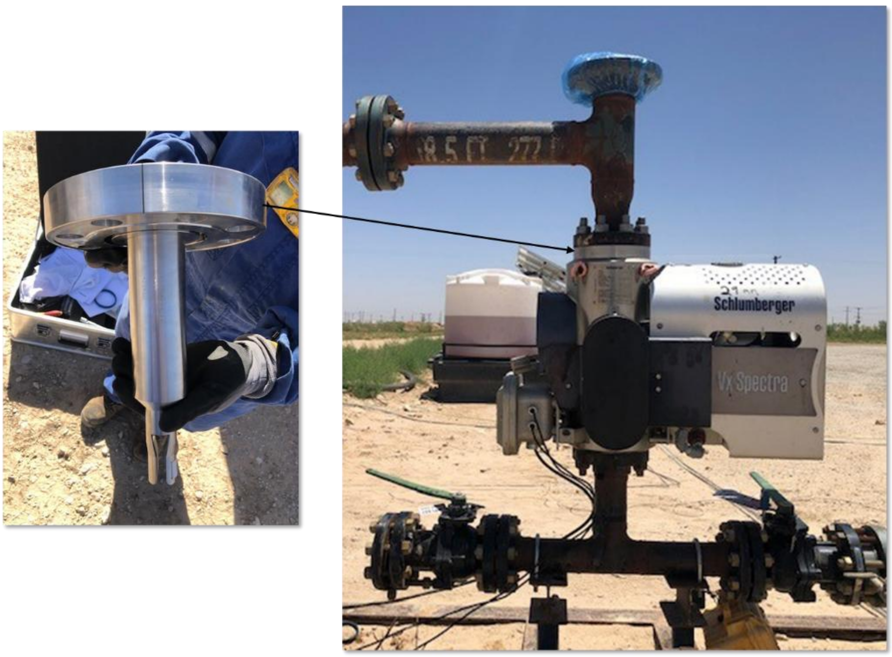

Figure 13 – Typical installation of MPFM equipped with XRF source and LRE in the Permian basin, Texas, US.

The increase of differential pressure for the same produced total mass flow rate is depicted in figure 14. From an average Δp of 130 mbar, the installation of the LRE increases it up to 800 mbar, not far from the Δp increase factor calculated with equation (11). The gas and oil flow rates temporal evolution and their comparison with the readings from the orifice plate and Coriolis meter, respectively, connected to a test separator, are shown in figure 15. During the test, the well production was irregular, with an average GVF starting from 92% and ending up to 97% after a stable period during the last month, with a slow by constant GVF increase. The week around Oct 23rd, the well was shut in, followed by a typical surge in liquid production, as shown by the sudden increase in the oil flow rate. Despite all these events, the relative deviations in both gas and oil flow rate measurements from the MPFM and the separator were largely within ±10% during more than 3 months of testing, as demonstrated by the ±10% error bars in both graphs of figure (16).

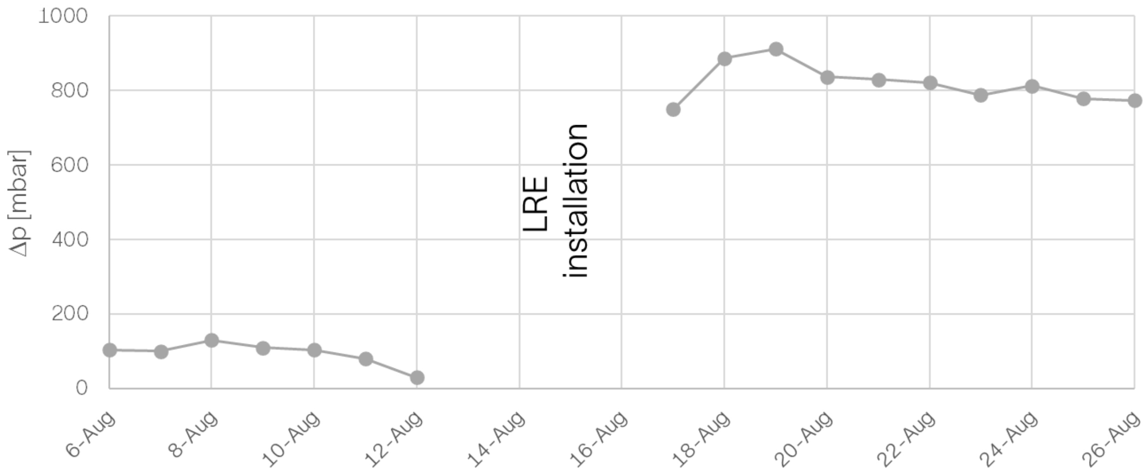

Figure 14 – Differential pressure across the MPFM before and after the installation of an LRE.

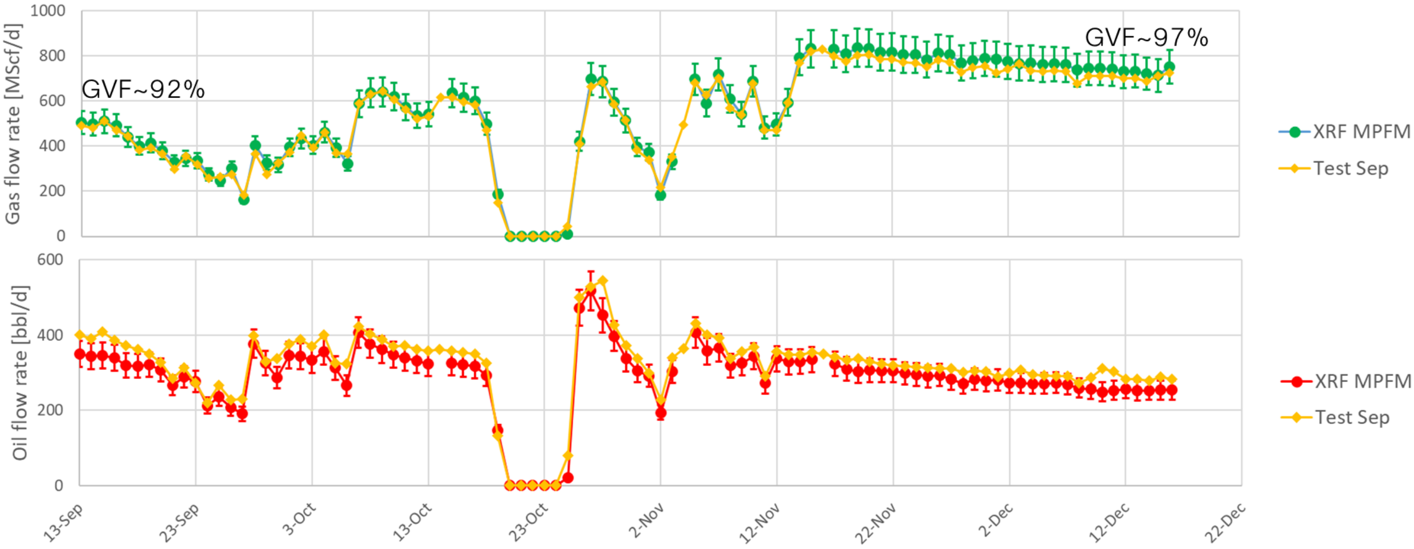

Figure 15 – Gas (top) and oil (bottom) flow rate from MPFM equipped with XRF source and LRE, for WLR from 21% to 13% and GVF from 92% to 97%. Error bars show the ±10% relative uncertainty of the daily production. Reference measurements from separator.

The second well tested with an MFPM equipped with XRF source and LRE is characterized by a stable production over more than 2 months. The well produced an average 35% WLR and average 92% GVF. Figure 16 presents the comparison between the measurements from an orifice plate for the gas phase and a Coriolis meter for the oil phase, with the output of the MPFM. Except for the week of Nov 29th when the line pressure was temporarily reduced from 35 bar to 17 bar, both monitoring from separator and MPFM are stable, with a slow decrease in both gas and oil flow rates. The measurement deviations between MPFM and separator are largely within ±5% over the entire duration of the test for both gas and oil flow rates.
The results of these tests in field conditions demonstrate the robustness and reliability of the XRF source and the LRE technologies, to improve the flow rate accuracy at high GVFs and maintain it throughout the lifecycle of unconventional wells.

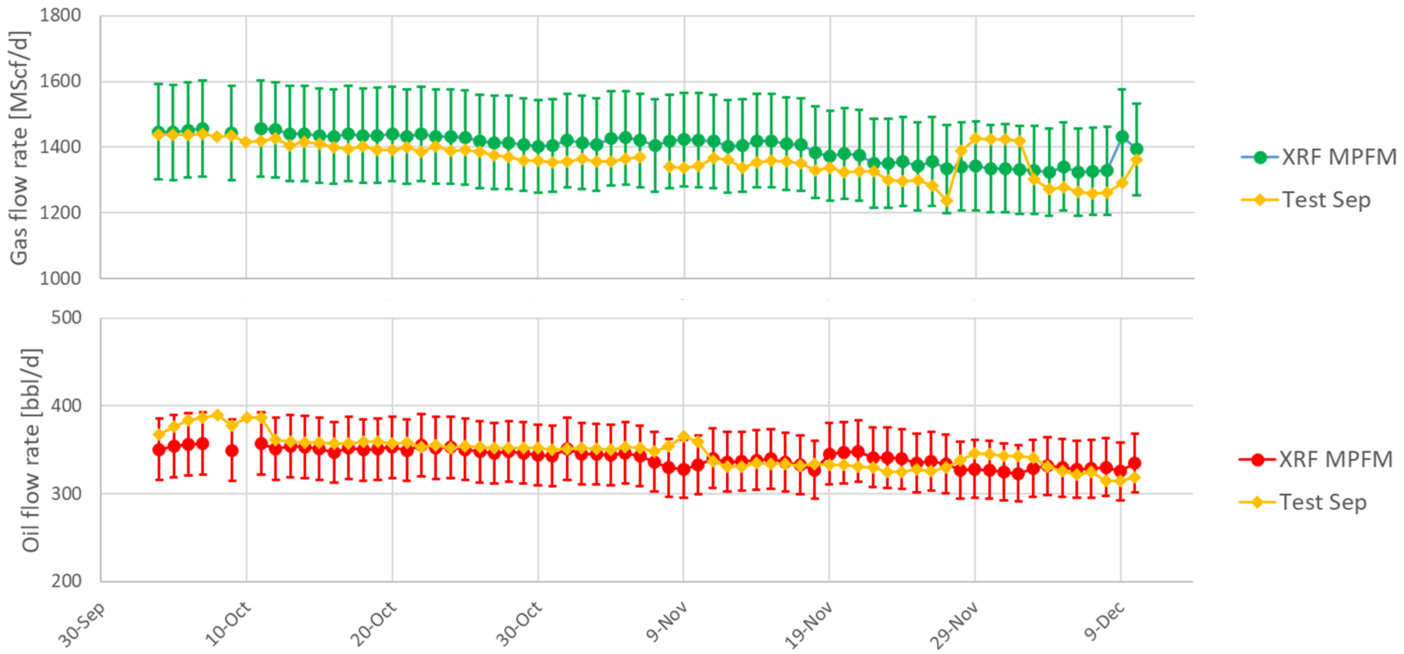

Figure 16 – Gas (top) and oil (bottom) flow rate from MPFM equipped with XRF source and LRE, for 35% WLR and 93% GVF. Error bars show the ±10% relative uncertainty of the daily production. Reference measurements from separator.

6 CONCLUSIONS

The XRF radioactive source and interpretation model for X- and γ-ray absorption MPFM enables obtaining accurate WLR and consequently oil flow rate measurements even for high-GVF high-WLR conditions typical of unconventional well production. The fluorescence X-rays emitted by the XRF source lead to cutting the WLR uncertainty by more than half for GVF > 95% when compared with an MPFM equipped with standard source, thus significantly improving the oil flow rate accuracy at levels required for fiscal allocation.
The LRE and updated multiphase flow model maintain the accuracy improvement throughout the lifecycle of unconventional wells, despite the rapid decline in production.
The XRF MPFM with LRE has been extensively validated in flow loop tests at in-house ISO-certified multiphase facility, successfully demonstrating high accuracy at high GVFs. The field exposure of the MPFMs equipped with the XRF source, fully compatible with the standard MPFM main body, and LRE has demonstrated the seamless retrofit of the existing deployed flowmeters and the significant improvement of WLR and oil flow rates, even under gas-lift slug-flow conditions and low mass flow rate. The workflow activity for the XRF MPFM with LRE is the same as for standard meters, thus requiring minimal additional training for deployment.
The high-accuracy XRF MPFM with LRE is leading to an increased new technology adoption in the US by replacing traditional bulky test separators equipped with natural gas−driven valves. This will help US oil and gas companies to achieve their sustainability goals through a significant emission reduction of greenhouse gases. Another possible application of the high-accuracy XRF MPFM is for wet-gas conventional wells, to help the energy transition through natural gas employed in blue hydrogen production.

7 ACKNOWLEDGMENTS

The authors would like to thank Dr. Cheng-Gang Xie and Guillaume Jolivet for fruitful discussions, the SLB North America Land team for the first field deployments of the XRF and LRE technologies, and SLB for permission to publish this paper.
The authors also acknowledge the local operators in the Permian basin who have trialed the XRF and LRE technologies in the field and provided access to the reference measurement data.

8 NOTATION

GVF Gas volume fraction
HE High energy
LE Low energy
LRE Low-rate Extender
MPFM Multiphase flowmeter
Std Standard
SWTC Singapore Well Testing Center
VLE Very low energy
WLR Water liquid ratio
XRF X-ray fluorescence
ω_k K-shell X-ray fluorescence yield

Subscripts
g gas
m mixture
o oil
w water

9 REFERENCES

[1] W. Lane, and R. Chokshi, 2014. *Considerations for Optimizing Artificial Lift in Unconventionals*. Paper presented at the Unconventional Resources Technology Conference, Denver, Colorado, USA, 25-27 August. URTeC-2014-1921823.

[2] EIA. 2018. *U.S. Crude Oil Production Efficiency Continues to Improve*. *Today in Energy*, 1 May. https://www.eia.gov/todayinenergy/detail.php?id=36012.

[3] Gristo, P. 2017. *Artificial Lift Overview and Perspectives for the Production of Unconventional Resources in the Neuquén Basin*. MS thesis. Heriot-Watt University, Edinburgh Scotland (March 2017). https://www.researchgate.net/publication/329681746_Artificial_Lift_overview_and_perspectives_for_the_production_of_unconventional_resources_in_the_Neuquen_basin.

[4] B. Singh, B. Gerrard, D. Reasoner, et al. 2022. *"Not Measured, Not Improved" Agile 3-Phase Well Flow Measurement and Well Testing Unit*. Paper presented at the Unconventional Resources Technology Conference, Houston, Texas, USA, 20–22 June. URTeC-2022-3719030.

[5] K. Moncada, L. Husoschi, B. Marnon, et al. 2024. *A New and Cost-Effective Way to Estimate Production in Unconventional Fields Using Advanced Multiphase Flowmeter Technology in North Dakota*. Paper presented at the Unconventional Resources Technology Conference held in Houston, Texas, USA, 17-19 June 2024. URTeC-2024-4054285.

[6] Y. Shumakov, B. Akbayev, M. Vigo, et al. 2014. Five Years' Experience Using Coriolis Separators in North Sea Well Testing. Paper presented at the Abu Dhabi International Petroleum Exhibition and Conference held in Abu Dhabi, UAE, 10–13 November 2014. SPE-171752-MS.

[7] Y. Pradhan, H. Xiong, J. Forrest, et al. 2018. *Additional Applications of Optimal Artificial Lift Strategies in the Permian Basin*. Presented at the Unconventional Resources Technology Conference, Houston, Texas, 23-25 July. URTeC-2018-2902293.

[8] B. Theuveny, K. Moncada, M. Roth, et al. 2019. *Large Deployment of Multiphase Flowmeters in an Unconventional Field*. Presented at the SPE Annual Technical Conference and Exhibition, Calgary, Alberta, Canada, 30 September -2 October. SPE-196129-MS.

[9] G. Falcone, G. F. Hewitt, C. Alimonti, et al. 2001. *Multiphase Flow Metering: Current Trends and Future Developments*. Paper presented at the SPE Annual Technical Conference and Exhibition, New Orleans, Louisiana, USA, 30 September-3 October. SPE-71474-MS.

[10] Pietro Fiorentini S.p.A. 2021. *Multiphase Flow Metering*. Accessed on 27 August 2025. https://www.fiorentini.com/wp-content/uploads/2021/03/mpfm_brochure_ENG.pdf.

Emerson Process Management 2022. *Roxar 2600 MPFM*. Accessed on 27 August 2025. https://www.emerson.com/documents/automation/product-data-sheet-roxar-2600-multiphase-flowmeter-rapid-adaptive-measurement-en-us-7260140.pdf.

[11] E. Delvaux, B. Germond, and N. K. Jha, 2004. *Combination of Dual-Energy Gamma Ray/Venturi Multiphase Flowmeter and Phase Splitter for Application in Very High Gas Volume Fraction Environment*. Paper presented at the Abu Dhabi International Petroleum Exhibition and Conference, Abu Dhabi, UAE., 10-13 October. SPE-88745-MS.

[12] M. Fiore, M. A. B. Razali, T. Zhang, et al. 2024. *Improving Multiphase Flowmeter Accuracy for Hydrocarbon Allocation and Wet Gas Production of Unconventional Oil-Gas Wells*. Paper presented at the International Petroleum Technology Conference, Dhahran, Saudi Arabia., 12-14 February. IPTC-23942-MS.

[13] G. F. Knoll 2000. *Radiation Detection and Measurement*, third edition. New York, Wiley and Sons.

[14] G. Yadigaroglu, G. F. Hewitt 2017. *Introduction to multiphase flow: basic concepts, applications and modelling*. Springer.

[15] J. W. Demmel 1997. *Applied Numerical Linear Algebra*. Philadelphia, Pennsylvania, USA: Society for Industrial and Applied Mathematics.

[16] R. Jenkins 2003. *X-Ray Analysis*. In *Encyclopedia of Physical Science and Technology*, third edition. Cambridge, Massachusetts, USA: Academic Press.

[17] M. Fiore, D. Chazal, and G. Jolivet 2020. *Radiation Source Device*. European Patent 2986974.

[18] J. E. Fernández and R. T. Mainardi 1986. *Thin-Film Thickness Calculation to Maximize X-Ray Fluorescence Intensity in Transmission Arrangements*. X-Ray Spectrometry **15**: 103-105.

[19] D. Chazal, M. Fiore, G. Jolivet, et al. 2014. *Enhancements in Fraction Measurements and Flow Modeling for Multiphase Flowmeters*. Paper presented at the SPE Annual Technical Conference and Exhibition, Amsterdam, The Netherlands, 27–29 October. SPE-170853-MS.

[20] D. Chazal, and M. Fiore 2021. *Spectral Analysis with Spectrum Deconvolution*. US patent 11029264.

[21] Euratom. 2013. *Council Directive 2013/59/Euratom of 5 December 2013 laying down basic safety standards for protection against the dangers arising from exposure to ionizing radiation*. https://eur-lex.europa.eu/eli/dir/2013/59/oj

[22] ISO 5167-4:2022. *Measurement of fluid flow by means of pressure differential devices inserted in circular cross-section conduits running full*. https://www.iso.org/standard/79181.html